

Neutrino neutral-current elastic scattering on ^{12}C

A. V. Butkevich¹ and D. Perevalov²

¹*Institute for Nuclear Research, Russian Academy of Sciences,
60th October Anniversary Prosp. 7A, Moscow 117312, Russia*

²*Fermi National Accelerator Laboratory; Batavia, IL 60510*

(Dated: February 16, 2022)

The neutral current elastic scattering of neutrinos on Carbon and CH_2 targets is computed using the relativistic distorted-wave impulse approximation with relativistic optical potential. Results for exclusive and inclusive neutrino reactions on ^{12}C target are presented. We show that the nuclear effects on the shape of four-momentum transferred squared distribution $d\sigma/dQ_{QE}^2$ in neutrino neutral-current and charged-current quasi-elastic scattering are similar. We also calculate flux-averaged neutral current elastic differential cross section $d\sigma/dQ_{QE}^2$ for neutrino scattering from CH_2 , as well as, the neutral-current to charged-current cross section ratio as functions of Q_{QE}^2 . The value of axial mass M_A is extracted from a fit of $d\sigma/dQ_{QE}^2$ cross section measured in MiniBooNE experiment. The extracted value of $M_A = 1.28 \pm 0.05$ GeV is consistent within errors with the MiniBooNE result. Additionally, for proton kinetic energies above the Cherenkov threshold, the strange quark contribution to the neutral current axial vector form factor at $Q_{QE}^2 = 0$, Δs , was extracted from a fit of MiniBooNE data for $\nu p \rightarrow \nu p$ to $\nu N \rightarrow \nu N$ cross section ratio. This value is found to be $\Delta s = -0.11 \pm 0.36$

PACS numbers: 25.30.-c, 25.30.Bf, 25.30.Pt, 13.15.+g

I. INTRODUCTION

Neutrino-nucleon neutral-current elastic (NCE) scattering provides an additional information about of structure of the hadronic weak neutral current (NC) and plays an important role in searching for the three active neutrino $\nu_{\text{active}} = \{\nu_e, \nu_\mu, \nu_\tau\}$ conversion to a sterile neutrino ν_s : a neutrino which has no coupling to neither W^\pm nor Z^0 bosons.

The weak neutral current of the nucleon may be parametrized in terms of two vector and

one axial-vector form factors. An additional induced pseudoscalar form factor is presented, but its contribution vanishes in the limit of a zero neutrino mass. In particular, the axial-vector form factor may be split into a non-strange and strange contributions. The latter one is proportional to the fraction of the nucleon spin carried by the strange quarks [1, 2]. Thus the axial-vector form factor is crucial for understanding the role that strange quarks play in determining the properties of nucleons.

In order to investigate how the strange quarks contribute to the observed properties of the nucleon various reactions have been proposed: deep inelastic scattering of neutrino or polarized charged leptons on proton [3, 4], and parity-violating electron scattering [5, 6]. The strange vector form factors were measured in parity-violating electron scattering experiments [7–11]. A combined analysis of these experiments data points to small strangeness of the vector form factors [12].

Whereas parity-violating electron scattering is sensitive to the electric and magnetic strangeness, neutrino-induced reactions are sensitive to the strange quark contribution Δs to the NC axial-vector form factor. A measurement of $\nu(\bar{\nu})$ -proton NCE at Brookhaven National Laboratory (BNL E734) [13] suggested a non-zero value of Δs . However, in Ref. [1] it has been shown that the BNL data cannot provide a decisive conclusion about the value of Δs when taking into account uncertainties in the vector strange form-factors. Moreover, this result suffers strongly from experimental uncertainties due to difficulties in determination of the absolute neutrino flux.

The measurement of the neutral-to-charged-current (CC) quasi-elastic cross section $R = NCE/CCQE$ in neutrino-nucleus scattering was proposed in Ref. [14] to extract information on the strange spin of the proton because much of the systematic uncertainty is canceled by using the ratio. An important effort in this direction was the MiniBooNE experiment, that measured the flux-averaged NCE differential cross section $d\sigma/dQ^2$ as a function of four-momentum transferred squared Q^2 and ratio $R = NCE/CCQE$ [15]. The MINERvA experiment [16] aims at high precision measurements of neutrino scattering cross sections, and would be well-suited to examine the Q^2 evaluation of strangeness form factor in NCE scattering.

Recently, the question about an additional sterile neutrino has drawn a considerable interest in the literature [18–20]. The short-baseline neutrino oscillation experiment, LSND, at the Los Alamos National Laboratory [17] reported evidence of $\bar{\nu}_\mu \rightarrow \bar{\nu}_e$ oscillation, but

with a squared mass difference Δm_{LSD}^2 that is inconsistent within a three neutrino mass model with the two other values extracted from solar, atmospheric, and reactor experiments, i.e. $\Delta m_{at}^2 + \Delta m_{sol}^2 \neq \Delta m_{LSD}^2$.

One of the most favorable scenarios that accommodates three independent Δm^2 values is an addition of a sterile neutrino. Because three active neutrinos couple to Z^0 , the rate of neutrino NC events should be unaffected by the three flavor neutrino oscillation. Conversely, an existence of a sterile neutrino adds a possibility of a $\nu_{active} \rightarrow \nu_s$ transition that would create a deficit in the rate of NC events.

However, the SNO experiment [21] made a neutral-current rate measurement and showed that the total flux of active neutrino from the Sun agree with expectation from the Standard Solar model. The Super-Kamiokande experiment excludes $\nu_\mu \rightarrow \nu_s$ and favors a pure $\nu_\mu \rightarrow \nu_\tau$ oscillation in its analysis of atmospheric neutrinos where an admixture of the two possibilities is allowed [22, 23]. The MINOS collaboration reported [24] the measurements of neutrino NC rates and spectra in an accelerator long baseline neutrino experiment. The rates at the near and far detectors are consistent with expectations from decay kinematics and geometry, providing new support for the interpretation of muon neutrino disappearance as oscillations among the three active neutrinos. So, an additional interest in the neutrino-nucleus NCE scattering cross section is that this process plays a key role in a search for the parameter space available for $\nu_{active} \rightarrow \nu_s$ oscillations.

It has been shown in Refs. [15, 25, 26] that in order to measure the strange quark contribution to the nucleon spin using a neutrino-nucleon NCE cross section it is necessary to distinguish $\nu p \rightarrow \nu p$ from $\nu n \rightarrow \nu n$ interactions. Otherwise, the total NCE cross-section on both proton and neutron ($\nu N \rightarrow \nu N$) has a negligible dependence on the nucleon spin's strangeness. A detailed analysis of the NCE scattering cross section's sensitivity to the strange content of nucleon neutral current was carried out in a relativistic plane-wave impulse approximation in Ref. [27].

Analysis of nuclear structure effects on the determination of the strange quark contribution in neutrino-nucleus NCE scattering were performed in Refs. [28, 29] where the relativistic Fermi Gas model (RFGM) and relativistic shell model including final state interaction (FSI) of outgoing nucleon were used. The effects of FSI were also studied in Ref. [30] within the RFGM and in Refs. [1, 31] in the framework of the Random Phase Approximation theory. The effects of FSI on the ratio of proton-to-neutron cross section in NCE scattering were

discussed in Refs.[28, 32, 33].

The effects of FSI on NCE scattering cross section were studied in Refs. [34–36] within the framework of a relativistic distorted-wave impulse approximation (RDWIA) with a relativistic optical potential. In Refs. [34, 35] important FSI effects arise from the use of optical potential within a relativistic Green’s function approach. An analysis of the sensitivity of NCE scattering cross section to the strangeness contribution was presented also in Refs.[37, 38] within the RDWIA and relativistic multiple-scattering Glauber approximation.

In this paper we present the RDWIA calculation of the neutrino-nucleon NCE scattering cross section on Carbon and CH_2 . In this approach that was successfully applied in Refs.[39–42] to CC quasi-elastic scattering we calculated the flux-averaged $d\sigma/dQ^2$ cross section and ratio $R(NCE/CCQE)$ and compare the results with the MiniBooNE data [15]. Additionally, the ratio of the predicted event rates in the MiniBooNE high energy $\nu p \rightarrow nup$ and $\nu N \rightarrow nuN$ event samples was calculated. This ratio is sensitive to the strange quark contribution to the nucleon spin, Δs . Using the MiniBooNE data for this distribution we performed a measurement of Δs and compared it to the MiniBooNE result reported in Ref. [15].

The outline of this article is as follows: In Sec. II we present briefly the formalism for the NCE scattering process and the RDWIA approach. The results are presented and discussed in Sec. III. Our conclusions are summarized in Sec. IV.

II. THE FORMALISM AND MODEL FOR THE NEUTRAL-CURRENT ELASTIC SCATTERING

In this section we consider the formalism for description of NCE exclusive

$$\nu(k_i) + A(p_A) \rightarrow \nu(k_f) + N(p_x) + B(p_B), \quad (1)$$

and inclusive

$$\nu(k_i) + A(p_A) \rightarrow \nu(k_f) + X \quad (2)$$

scattering off nuclei in the one- Z^0 -boson exchange approximation. Here $k_i = (\varepsilon_i, \mathbf{k}_i)$ and $k_f = (\varepsilon_f, \mathbf{k}_f)$ are the initial and final lepton momenta, $p_A = (\varepsilon_A, \mathbf{p}_A)$, and $p_B = (\varepsilon_B, \mathbf{p}_B)$ are the initial and final target momenta, $p_x = (\varepsilon_x, \mathbf{p}_x)$ is the ejectile nucleon momentum, $q = (\omega, \mathbf{q})$ is the momentum transfer carried by the virtual Z^0 -boson, and $Q^2 = -q^2 = \mathbf{q}^2 - \omega^2$

is the Z^0 -boson virtuality. As the basic outline follows closely the CC formalism developed in Ref. [39], we present a brief review that focuses on those modifications that arise from the weak neutral current.

A. Neutrino-nucleus NCE scattering cross sections

In the laboratory frame, the differential cross section for the exclusive (anti-)neutrino NCE scattering, in which only a single discrete state or narrow resonance of the target is excited, can be written as

$$\frac{d^5\sigma^{(nc)}}{d\varepsilon_f d\Omega_f d\Omega_x} = R \frac{|\mathbf{p}_x| \varepsilon_x}{(2\pi)^5} \frac{|\mathbf{k}_f|}{\varepsilon_i} \frac{G^2}{2} L_{\mu\nu}^{(nc)} W^{\mu\nu(nc)}, \quad (3)$$

where Ω_f is the solid angle for the lepton momentum, Ω_x is the solid angle for the ejected nucleon momentum, R is the recoil factor, $G \simeq 1.16639 \times 10^{-11} \text{ MeV}^{-2}$ is the Fermi constant, $L_{\mu\nu}^{(nc)}$ and $W_{\mu\nu}^{(nc)}$ are NC lepton and nuclear tensors, respectively.

The energy ε_x is the solution to the equation

$$\varepsilon_x + \varepsilon_B - m_A - \omega = 0, \quad (4)$$

where $\varepsilon_B = \sqrt{m_B^2 + \mathbf{p}_B^2}$, $\mathbf{p}_B = \mathbf{q} - \mathbf{p}_x$, $\mathbf{p}_x = \sqrt{\varepsilon_x^2 - m^2}$, and m_A , m_B , and m are masses of the target, recoil nucleus and nucleon, respectively. The missing momentum p_m and missing energy ε_m are defined by

$$\mathbf{p}_m = \mathbf{p}_x - \mathbf{q} \quad (5a)$$

$$\varepsilon_m = m + m_B - m_A \quad (5b)$$

From Eq.(4) the total energy of the ejected nucleon is given by

$$\varepsilon_x = \omega + m_A - \varepsilon_B \approx \omega + m - (\varepsilon_m - p_m^2/2m_B) \quad (6)$$

and the nucleon kinetic energy can be written as

$$T_N = \omega - (\varepsilon_m - p_m^2/2m_B) \approx \omega - \varepsilon_m, \quad (7)$$

if one neglects the recoil nucleon energy $p_m^2/2m_B$. As the outgoing neutrino is undetected the differential cross section Eq.(3) can be rewritten in “no-recoil” approximation as follows

$$\frac{d^5\sigma^{(nc)}}{dT_N d\Omega_f d\Omega_x} \approx \frac{d^5\sigma^{(nc)}}{d\varepsilon_f d\Omega_f d\Omega_x} \quad (8)$$

The leptonic tensor $L_{\mu\nu}^{(nc)}$ is separated into symmetric and antisymmetric components that are given as in Ref. [39]. Note, that the weak lepton NC is conserved for massless neutrino and $q^\mu L_{\mu\nu}^{(nc)} = L_{\mu\nu}^{(nc)} q^\nu = 0$. All the nuclear structure information and FSI effects are contained in the weak NC nuclear tensor $W_{\mu\nu}^{(nc)}$, which is given by the bilinear product of the transition matrix elements of the nuclear NC operator $J_\mu^{(nc)}$ between the initial nucleus state $|A\rangle$ and the final state $|B_f\rangle$ as

$$W_{\mu\nu}^{(nc)} = \sum_f \langle B_f, p_x | J_\mu^{(nc)} | A \rangle \langle A | J_\nu^{(nc)\dagger} | B_f, p_x \rangle, \quad (9)$$

where the sum is taken over undetected states. This tensor is an extremely complicated object as, in principle, the exact form for many body wave functions and operators must be used. A general model-independent covariant form of $W_{\mu\nu}^{(nc)}$ and the result of its contraction with the leptonic tensor were obtained in Ref. [27]. There it was shown that the contraction $L_{\mu\nu}^{(nc)} W^{\mu\nu(nc)}$ and therefore the differential cross section in Eq. (3) is completely determined by a set of eight structure functions.

General expressions for the cross sections of the exclusive and inclusive CCQE neutrino scattering off nucleus are given in Ref. [39] in terms of weak response functions. In order to apply these expressions for calculation of neutrino-nucleus NCE scattering cross sections it is necessary to replace $G^2 \cos^2 \theta_C \rightarrow G^2$, express the response functions as suitable combinations of the hadron tensor components $W_{\mu\nu}^{(nc)}$, and calculate the coefficient v_i for massless neutrino. The single differential cross section as a function of the outgoing nucleon's kinetic energy T_N can be obtained after performing integration of the cross section in Eq.(8) over solid angles of the outgoing neutrino and nucleon.

B. Model

We describe the neutrino-nucleon NCE scattering in the impulse approximation, assuming that the incoming neutrino interacts with only one nucleon, which is subsequently emitted, while the remaining $(A-1)$ nucleons in the target are spectators. When the nuclear current is written as the sum of single-nucleon currents, the nuclear matrix element in Eq.(9) takes the form

$$\langle p, B | J^{\mu(nc)} | A \rangle = \int d^3r \exp(i\mathbf{t} \cdot \mathbf{r}) \bar{\Psi}^{(-)}(\mathbf{p}, \mathbf{r}) \Gamma^{\mu(nc)} \Phi(\mathbf{r}), \quad (10)$$

where $\Gamma^{\mu(nc)}$ is the NC vertex function, $\mathbf{t} = \varepsilon_B \mathbf{q}/W$ is the recoil-corrected momentum transfer, $W = \sqrt{(m_A + \omega)^2 - \mathbf{q}^2}$ is the invariant mass, Φ and $\Psi^{(-)}$ are the relativistic bound-state and outgoing wave functions.

The single-nucleon charged current has a $V-A$ structure $J^{(nc)\mu} = J_V^{\mu(nc)} + J_A^{\mu(nc)}$. For a free-nucleon vertex function, $\Gamma^{\mu(nc)} = \Gamma_V^{\mu(nc)} + \Gamma_A^{\mu(nc)}$, we use the vector current vertex function

$$\Gamma_V^{\mu(nc)} = F_V^{(nc)}(Q^2)\gamma^\mu + i\sigma^{\mu\nu}q_\nu F_M^{(nc)}(Q^2)/2m, \quad (11)$$

and the axial current vertex function

$$\Gamma_A^{\mu(nc)} = F_A^{(nc)}(Q^2)\gamma^\mu\gamma_5 + F_P^{(nc)}(Q^2)q^\mu\gamma_5. \quad (12)$$

The vector form factors $F_i^{(nc)}$ ($i = V, M$) are related to the corresponding electromagnetic ones for proton F_i^p and neutron F_i^n , plus a possible isoscalar strange-quark contribution F_i^s , i.e. [2]

$$F_V^{(nc)} = \tau_3(0.5 - \sin^2\theta_W)(F_1^p - F_1^n) - \sin^2\theta_W(F_1^p + F_1^n) - F_V^s/2 \quad (13a)$$

$$F_M^{(nc)} = \tau_3(0.5 - \sin^2\theta_W)(F_2^p - F_2^n) - \sin^2\theta_W(F_2^p + F_2^n) - F_M^s/2, \quad (13b)$$

where $\tau_3 = +(-1)$ for proton (neutron) knockout and θ_W is the Weinberg angle ($\sin^2\theta_W \approx 0.2313$). The axial $F_A^{(nc)}$ form factor is expressed as

$$\Gamma_A^{\mu(nc)} = (\tau_3 F_A - F_A^s)/2, \quad (14)$$

where F_A^s describes possible strange-quark contributions. In this work we neglect the strangeness contributions, i.e., it is supposed that $F_V^s = F_M^s = F_A^s = 0$. For the nucleon form factors $F_i^{p(n)}$ the approximation of Ref. [43] is used. Because the bound nucleons are the off-shell we employ the de Forest prescription [44] and Coulomb gauge for off-shell vector current vertex Γ_V^μ . The vector-axial form factor is parametrized as a dipole with the axial nucleon mass M_A , which controls the Q^2 dependence of F_A .

The independent particle shell model (IPSM) is assumed in the calculations of the nuclear structure, taking into account the short-range nucleon-nucleon (NN) correlation in the ground state. According to the experimental data [45, 46] the occupancy of the IPSM orbitals of ^{12}C equals on average 89%. We assume that the missing strength (11%) can be attributed to the NN correlations, leading to the appearance of the high-momentum and

high-energy component in the nucleon distribution in the target. To estimate this effect in the inclusive cross sections, we consider a phenomenological model that incorporates both the single-particle nature of the nucleon spectrum at low energy (IPSM orbitals) and the high-energy and high-momentum components due to NN correlations.

For ^{12}C we use the same relativistic wave functions of the bound nucleon states Φ as in Refs.[41, 42]. The wave functions were obtained from Ref. [47] as the self-consistent solutions of the relativistic Hartree-Bogoliubov equations, derived within a relativistic mean field approach. The normalization factors $S(\alpha)$ relative to the full occupancy of the IPSM orbitals of ^{12}C [45, 46] are: $S(1p_{3/2})=84\%$, $S(1s_{1/2})=100\%$ with an average factor of about 89%.

In order to take into account FSI effects in the RDWIA, the distorted-wave function, Ψ , is evaluated as a solution of the Dirac equation containing a phenomenological relativistic optical potential. The channel coupling in the FSI [48] of the $N + B$ system is taken into account. The relativistic optical potential consists of a real part which describes rescattering of the ejected nucleon and an imaginary part that accounts for its absorption into unobserved channels. We use the LEA program [49] for the numerical calculation of the distorted wave functions with the EDAD1 parametrization [50] of the relativistic optical potential for Carbon. This code, initially designed for computing exclusive electron-nucleus scattering, was successfully tested against $A(e, e'p)$ data [45, 51], and adopted for neutrino reactions [39].

A complex optical potential with a nonzero imaginary part generally produces an absorption of the flux. For the exclusive $A(l, l'N)$ channel this reflects the coupling between different open reaction channels. However, for the inclusive reaction, the total flux must be conserved. In Refs. [52, 53], it was shown that the inclusive CCQE neutrino cross section of the exclusive channel $A(l, l'N)$ calculated with only the real part of the optical potential is almost identical when calculated via the Green's function approach [52], in which the FSI effects on inclusive reaction $A(l, l'X)$ are treated by means of a complex potential, and the total flux is conserved. We calculate the inclusive $d\sigma/dQ^2$ sections with the EDAD1 relativistic optical potential in which only the real part is included. The inclusive cross sections with FSI effects in the presence of short-range NN correlations were calculated using the method proposed in Ref. [39].

III. RESULTS AND DISCUSSION

A. Neutral Current Elastic differential cross section

The exclusive reaction $\nu + A \rightarrow \nu + p + B$ reaction is a good signal sample of (anti)neutrino NCE scattering off nuclei. The measurement of the range of the scattered proton, its angle with respect to the direction of the incident neutrino θ_p , and its rate of energy loss allow to identify the particle as a proton and determine proton kinetic energy T_p . In impulse approximation, assuming the target nucleon to be at rest inside nucleus, these measured quantities ($T_p, \cos \theta_p$) determine the neutrino energy through the kinematic relation

$$\varepsilon_\nu = \frac{m_p}{\cos \theta_p (1 + 2m_p/T_p)^{1/2} - 1}, \quad (15)$$

where m_p is the proton mass. In neutrino oscillation experiments with two detectors the spectra of the protons as functions of neutrino energies, measured at near and far detectors can be used to search for $\nu_{active} \rightarrow \nu_s$ transition that would create a deficit in the rate of one proton events at far detector. Note, that precise measurement of the (anti)neutrino NCE scattering off neutron appear problematic due to the difficulties associated with neutron detection. In Figs.1, 2, and 3 the (anti)neutrino NCE exclusive cross sections $\sigma_P = d\sigma_p/dT_p$ (per bound proton), $\sigma_n = d\sigma_n/dT_n$ (per bound neutron), and sum $\sigma_p + \sigma_n$ are displayed as functions of the emitted nucleon kinetic energy for proton, neutron, and proton or neutron knockout, respectively. The calculations correspond to Carbon target and incoming energies of 500 MeV and 1000 MeV. The upper (lower) panels show the cross sections for neutrino (antineutrino) NCE scattering in comparison with results obtained in Refs.[34, 37]. These cross sections were also calculated in the RDWIA approach with dipole approximation of the nucleon form factors, EDAD1 parametrization of relativistic optical potential and neglecting the NN correlations in the ground state of Carbon. We observe that our calculations and those performed in the framework of RDWIA formalism are in a good agreement. For neutrino (antineutrino) the σ_p/σ_n NCE cross section ratio increases almost linearly with nucleon energy: from ≈ 0.7 (≈ 0.7) for $T_N \approx 20 - 50$ MeV up to ≈ 0.82 (≈ 2) for $T_N = 700$ MeV.

To study the nuclear effects on the Q^2 distribution, we calculated (with $M_A = 1.032$ GeV and $F_A^s = 0$) the inclusive cross sections $(d\sigma/dQ^2)_{nuc}$ (per bound nucleon) of the neutrino NCE scattering on Carbon. The results for neutrino energies $\varepsilon_\nu = 0.5, 0.7, 1.2$ and 2.5 GeV

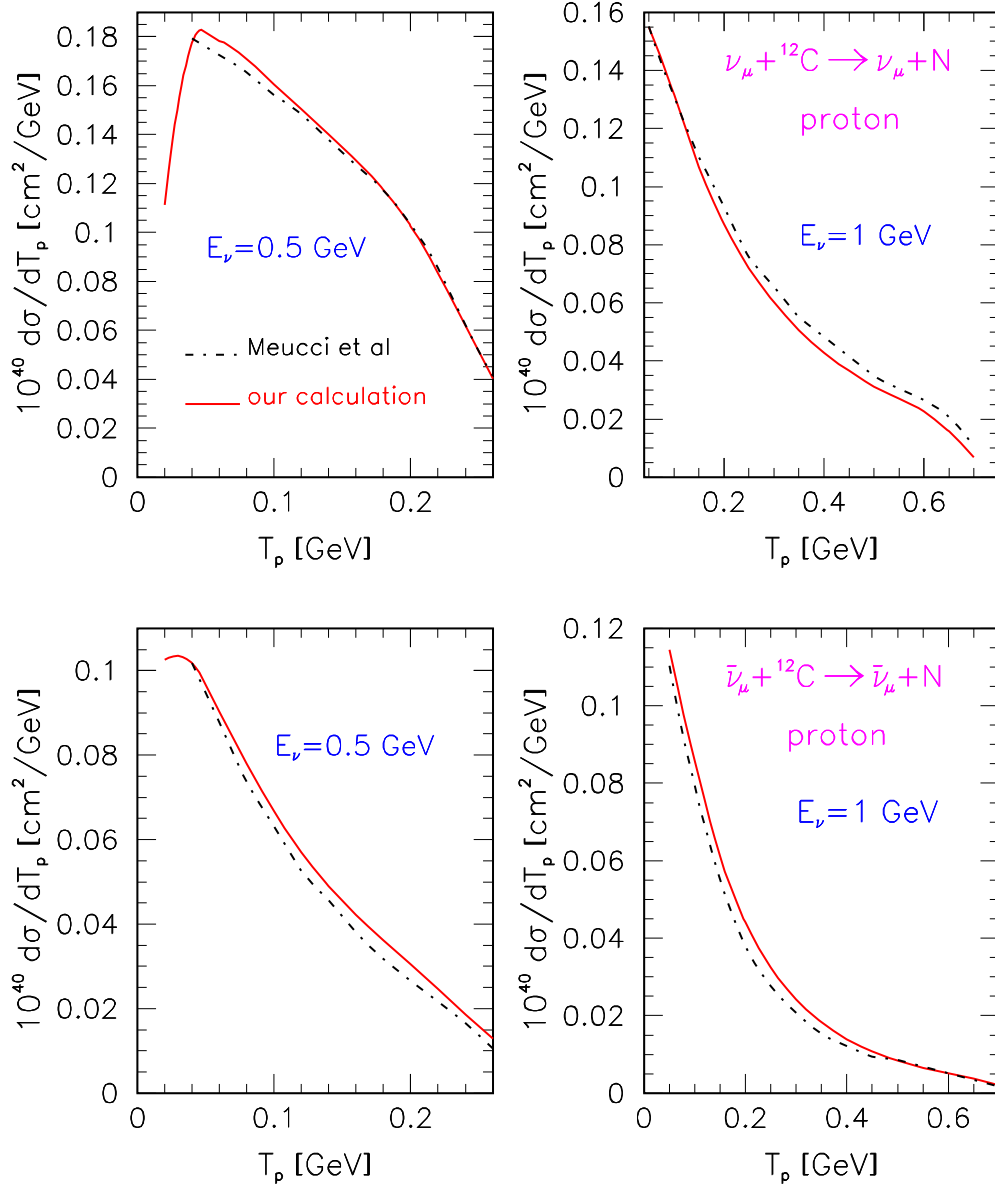


FIG. 1: (Color online) Differential cross sections σ_p of neutrino (upper panel) and antineutrino (lower panel) NCE scattering as a function of the outgoing proton kinetic energy for two the values of incoming (anti)neutrino energy: $\varepsilon_\nu = 500$ and 1000 MeV, calculated in the RDWIA. The solid lines represent the results obtained in this work and the dot-dashed lines are the results of Ref. [34].

are shown in Fig.4 in comparison with cross section for neutrino NCE scattering on a free nucleon $(d\sigma/dQ^2)_{free} = 0.5[(d\sigma/dQ^2)_p + (d\sigma/dQ^2)_n]$, where $(d\sigma/dQ^2)_p$ and $(d\sigma/dQ^2)_n$ are the cross sections for neutrino NCE scattering on free proton and neutron, respectively.

Nuclear effects on the shape of the Q^2 distribution, i.e., ratios $R(\varepsilon_\nu, Q^2) =$

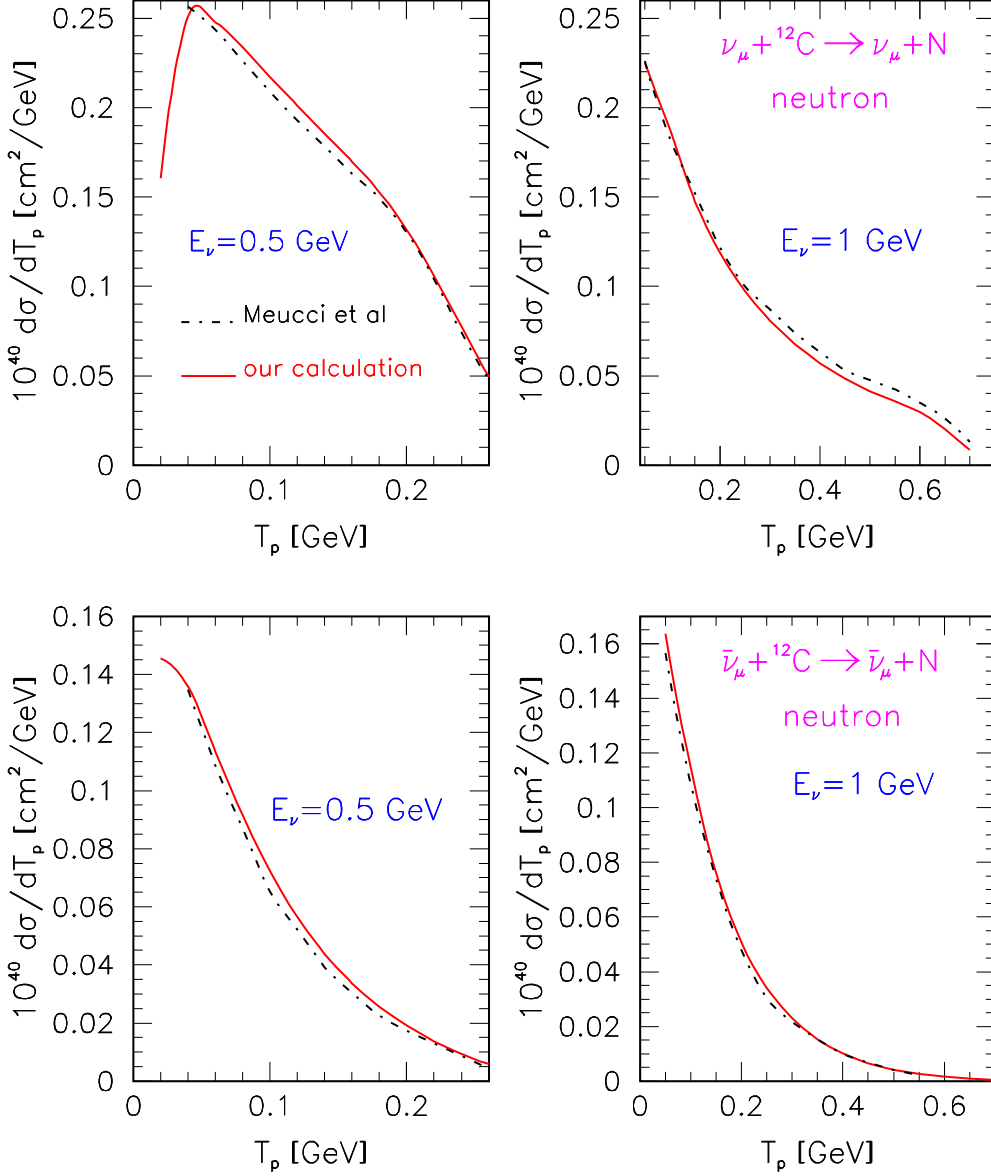


FIG. 2: (Color online) The same as Fig.1, but for neutron knockout (σ_n).

$(d\sigma/dQ^2)_{nuc}/(d\sigma/dQ^2)_{free}$ are presented in Fig.5. The results obtained for neutrino energies $\varepsilon_\nu = 0.5, 0.7, 1.2$ and 2.5 GeV are compared with those calculated for neutrino CCQE scattering in Ref. [41]. We observe that nuclear effects in neutrino NCE and CCQE scattering, in general, are similar. The nuclear effects are seen at low Q^2 ; the tail of the momentum distribution at high Q^2 , an overall suppression, and slight change in slope in the middle region at $\varepsilon_\nu \geq 1$ GeV is also observed. The range of Q^2 where $R \approx 1$ (i.e., nuclear effects are small and therefore cannot affect the measurement of the effective M_A) increases with

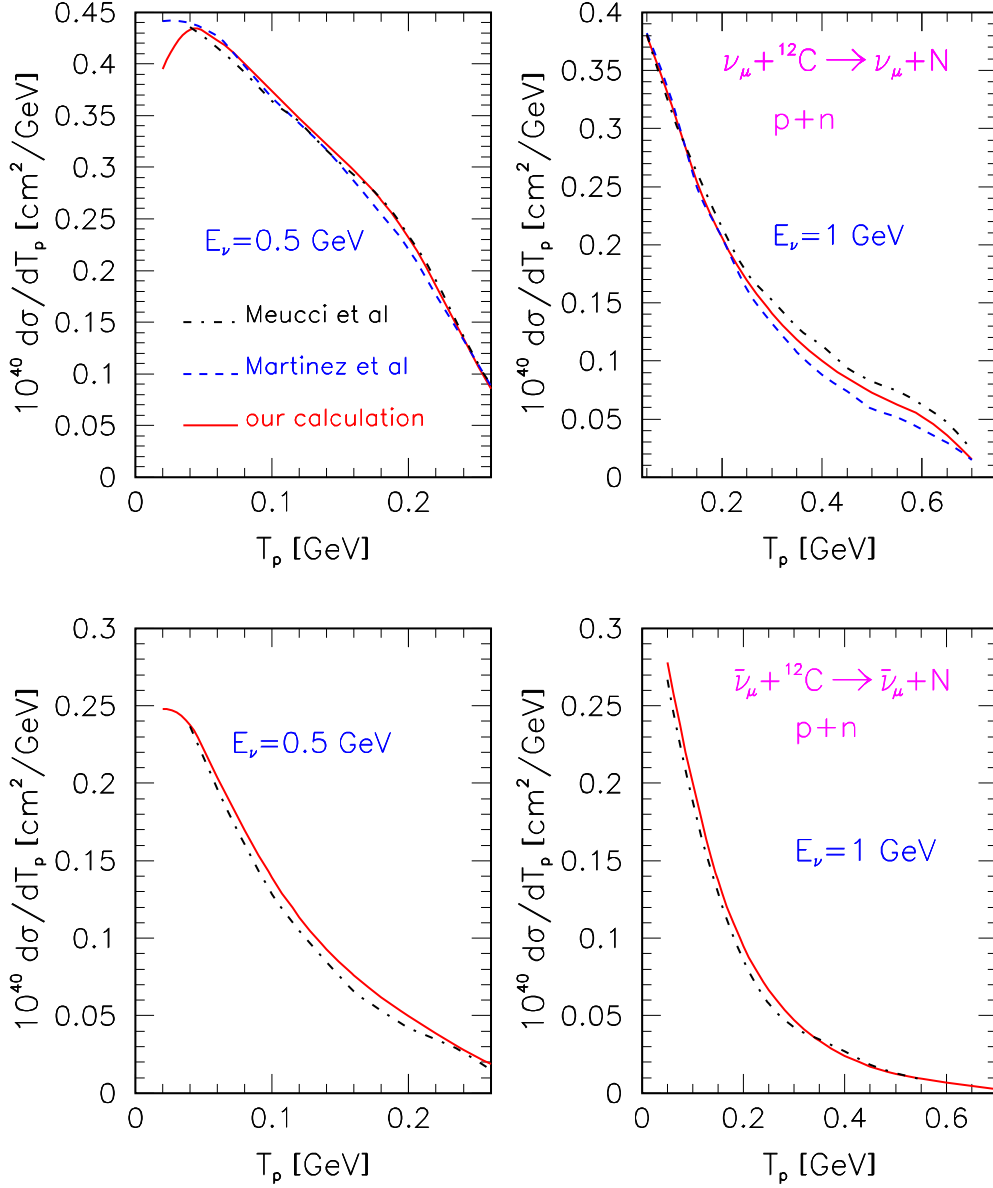


FIG. 3: (Color online) The same as Fig.1, but for proton or neutron knockout ($\sigma_p + \sigma_n$). The dashed lines show the RDWIA results of Ref. [37].

the incoming neutrino energy.

The measurement of the neutral-to-charged-current cross sections ratio in the neutrino-nucleus scattering was proposed in Ref. [14] to extract a possible strange-quark contribution. Our RDWIA results for $R = NC/CC = (d\sigma/dQ^2)^{NC}/(d\sigma/dQ^2)^{CC}$ ratio, obtained with $M_A = 1.032$ GeV and $F_A^s = 0$ are presented in Fig.6 as functions of Q^2 for neutrino energies $\varepsilon = 0.5, 0.6, 1.2$ and 2.5 GeV. The inclusive CCQE cross sections $(d\sigma/dQ^2)^{CC}$ were

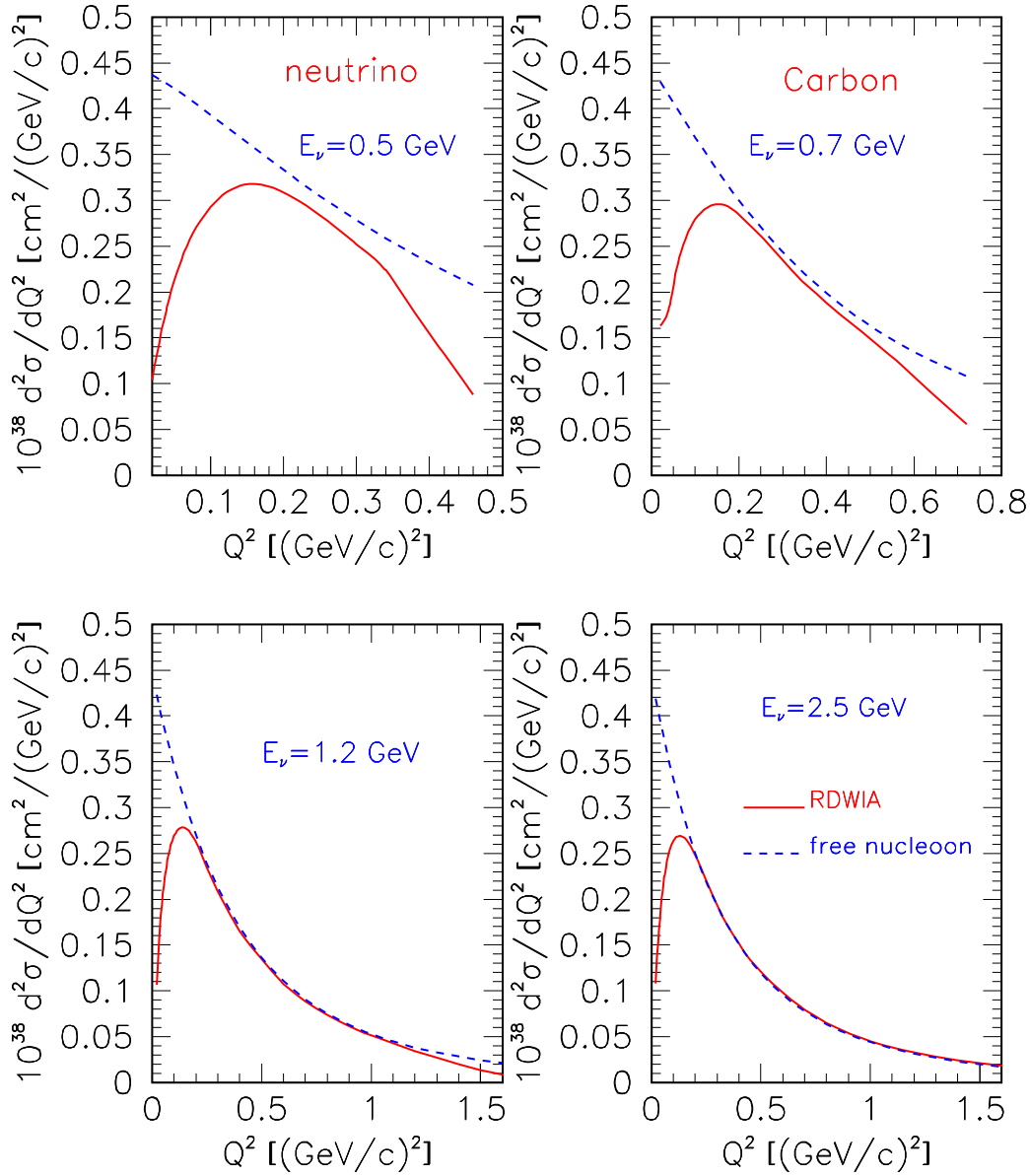


FIG. 4: (Color online) Inclusive NCE cross sections vs. the four-momentum transfer Q^2 for neutrino scattering off ^{12}C (solid line) and free nucleon (dashed line) and for the four values of incoming neutrino energy: $\varepsilon = 0.5, 0.7, 1.2$ and 2.5 GeV .

in Ref. [41]. The NC/CC ratio decreases as Q^2 increases from ~ 1.9 at $Q^2 \approx 0.1 (\text{GeV}/c)^2$ and reaches the minimum at large value of Q^2 . The fact that the CCQE cross section goes to zero more rapidly than the corresponding NCE one (due to the muon mass) causes the enhancement of the ratio at large value of Q^2 close to the upper border of the allowed kinematic range of Q^2 . The results obtained in Refs.[34, 37] show similar features.

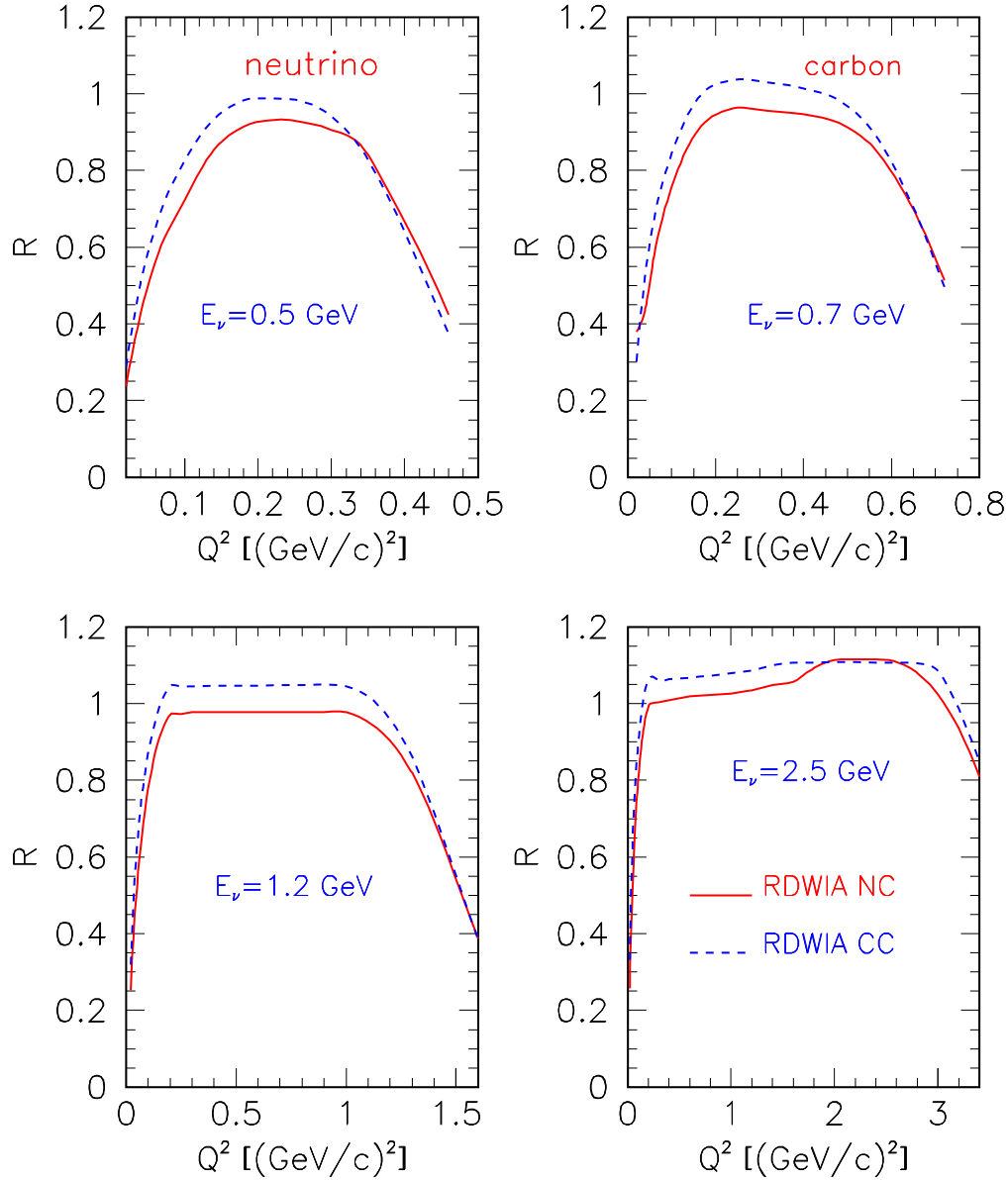


FIG. 5: (Color online) Ratio $R(\varepsilon_\nu, Q^2)$ vs. the four-momentum transfer Q^2 for neutrino scattering off ^{12}C and for the four values of incoming neutrino energy: $\varepsilon = 0.5, 0.7, 1.2$ and 2.5 GeV. As shown in the key, the ratios were calculated for neutrino NCE and CCQE scattering.

B. MiniBooNE flux-averaged differential cross section: comparison with data

The MiniBooNE collaboration reported [15] high-statistic measurement of the flux-averaged NCE differential cross section for neutrino scattering on CH_2 as a function of Q_{QE}^2 . In this experiment the sum of kinetic energies of all final state nucleons that are pro-

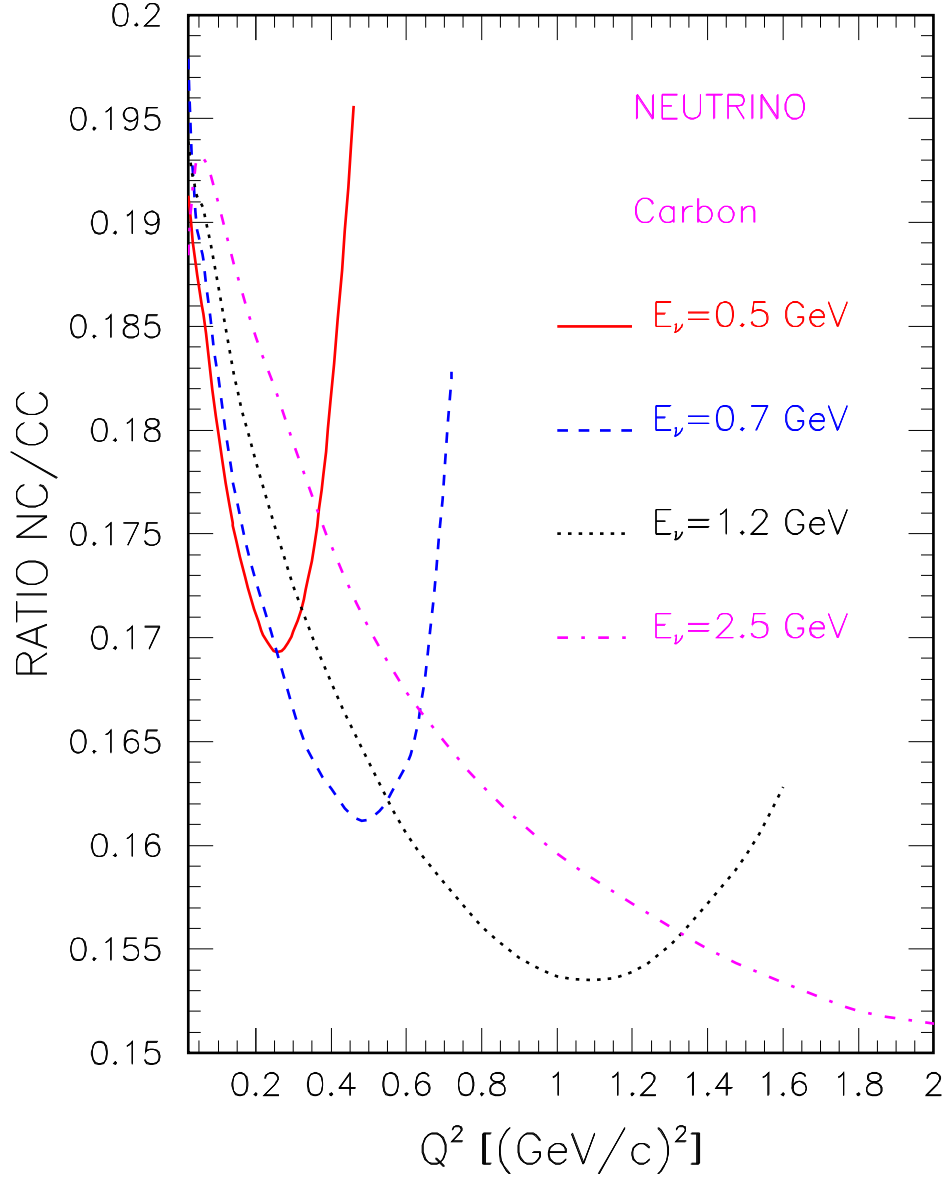


FIG. 6: (Color online) Ratio of neutral-to-charged-current cross sections $R = NC/CC$ vs. the four-momentum transfer Q^2 for neutrino scattering off ^{12}C and for the four values of incoming neutrino energy: $\varepsilon = 0.5, 0.7, 1.2$ and 2.5 GeV.

duced in the interaction $T = \sum_i T_i$ was measured and spectrum of NCE events dN_{NCE}/dT was reconstructed as a function $T \approx \omega$. Assuming that the target nucleon is at rest, Q_{QE}^2 was determined for each event as

$$Q_{QE}^2 = 2mT = 2m \sum_i T_i. \quad (16)$$

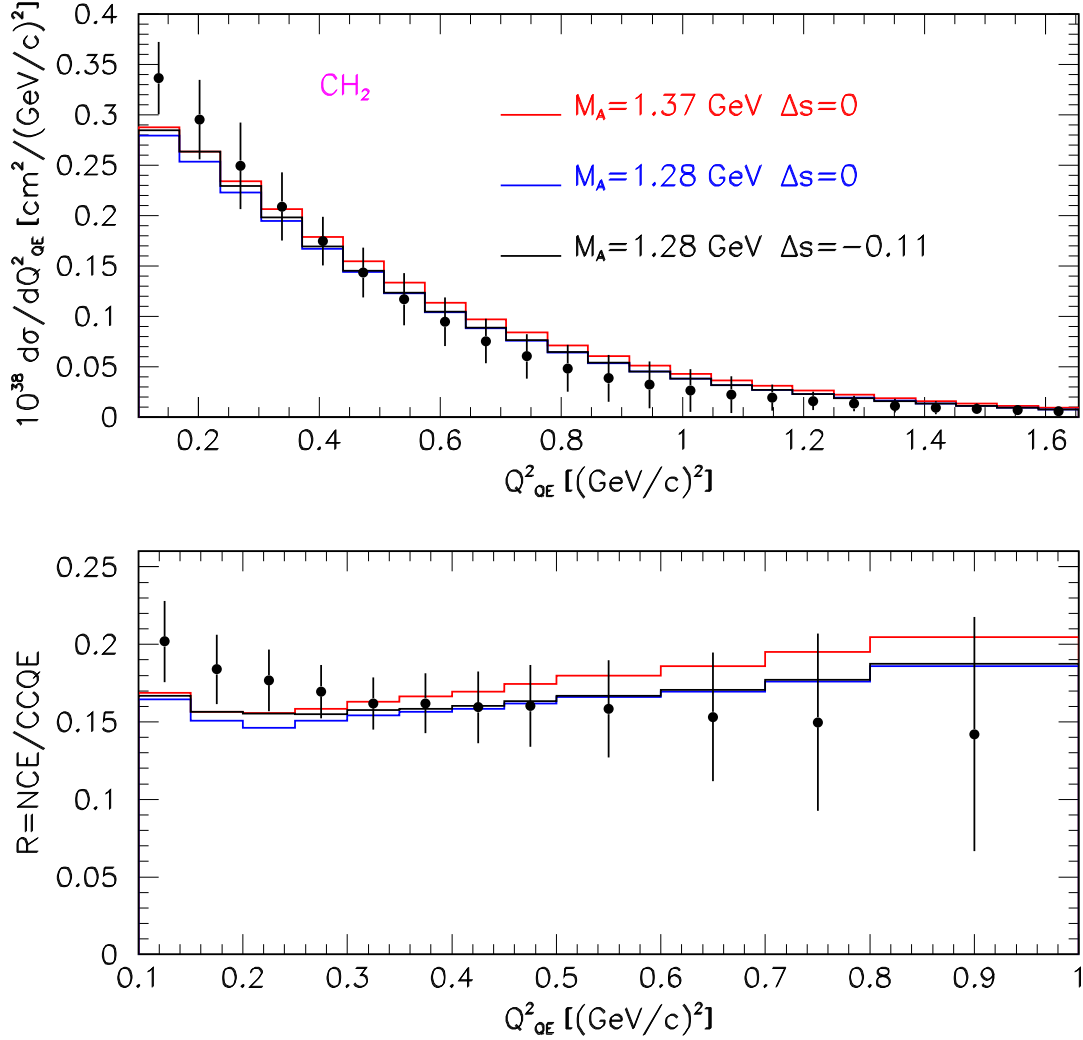


FIG. 7: (Color online) Flux-averaged $d\sigma/dQ_{QE}^2$ cross section per nucleon (upper panel) for neutrino scattering on CH_2 and $NCE/CCQE$ cross section ratio (lower panel) as a function of Q_{QE}^2 . The NCE cross section and $CCQE/NCE$ ratio calculated with values of $M_A = 1.28$ GeV (blue line), 1.37 GeV (red line), both with the value $\Delta s = 0.0$. Also shown is the strange quark effect on the NCE cross-section and the ratio with a value of $\Delta s = -0.11$ and $M_A = 1.28$ GeV (black line). The MiniBooNE data are shown as points.

MiniBooNE reported the NCE differential cross section in the range of Q_{QE}^2 from 0.1 to about 1.65 (GeV/c)^2 . This differential cross section distribution was fitted with a dipole axial form factor and best fit for $M_A = 1.39 \pm 0.11 \text{ GeV}$ was obtained. Using the data from charged-current neutrino interaction sample, the $NCE/CCQE$ cross sections ratio as a function of Q_{QE}^2 was measured. One should understand that, in fact, the NCE flux-averaged differential cross section $d\sigma/dT$ was measured, which under the assumption of a scattering on free nucleon, was recalculated as $d\sigma/dQ_{QE}^2 = (d\sigma/dT)/2m$. The details of the unfolding procedure in measurement of the cross section can be found in Ref. [25].

We calculated the NCE flux-averaged inclusive $\langle d\sigma_{NCE}/dT \rangle$ cross section in the framework of RDWIA approach that was recalculated as $\langle d\sigma_{NCE}/dQ_{QE}^2 \rangle = \langle d\sigma_{NCE}/dT \rangle / 2m$. The details of the calculation $\langle d\sigma_{NCE}/dT \rangle$ cross section are described in Appendix A. To extract a value for the parameter M_A we calculated this cross section with the Booster Neutrino Beamline flux [54] using the Q_{QE}^2 bins $\Delta Q^2 = Q_{i+1}^2 - Q_i^2$ similar to [15]

$$\left(\frac{d\sigma}{dQ_{QE}^2} \right)_i = \frac{1}{\Delta Q^2} \int_{Q_i^2}^{Q_{i+1}^2} \left\langle \frac{d\sigma}{dQ_{QE}^2}(Q_{QE}^2) \right\rangle dQ_{QE}^2 \quad (17)$$

and NCE to CCQE cross section ratio

$$R_i = NCE/CCQE = (d\sigma_{NCE}/dQ_{QE}^2)_i / (d\sigma_{CC}/dQ^2)_i, \quad (18)$$

The CCQE differential cross section $d\sigma_{CC}/dQ^2$ was calculated in the RDWIA approach in Ref. [42]. The fit to the extracted flux-averaged $\langle d\sigma_{NCE}/dQ_{QE}^2 \rangle$ yield the parameter $M_A = 1.28 \pm 0.5 \text{ GeV}$. Fig.7 shows the MiniBooNE measured flux-averaged differential $d\sigma_{NCE}/dQ_{QE}^2$ cross section and $R = NCE/CCQE$ ratio [15] as a function of Q_{QE}^2 compared with the RDWIA calculations with the value of $M_A = 1.28 \text{ GeV}$. The result obtained with $M_A = 1.37 \text{ GeV}$, that was extracted in Ref. [42] from the fit to measured in Ref. [55] flux-integrated CCQE cross section $d\sigma_{CC}/dQ^2$, also is shown.

There is an overall agreement within errors between the RDWIA predictions and the MiniBooNE data at high Q_{QE}^2 . However one should note that at $Q_{QE}^2 \geq 0.4 \text{ (GeV/c)}^2$ the inclusive cross section, as well as, $R = NCE/CCQE$ ratio, calculated with the value of $M_A = 1.28 \text{ GeV}$ has a better agreement with data. At $Q_{QE}^2 < 0.25 \text{ (GeV/c)}^2$ the calculation underestimate both cross section and the NCE/CCQE ratio by 17% or less.

**C. MiniBooNE $\nu p \rightarrow \nu p/\nu N \rightarrow \nu N$ differential cross section cross-section ratio:
comparison with data**

In addition to the $\nu N \rightarrow \nu N$ differential cross-section, MiniBooNE has published the $\nu p \rightarrow \nu p$ to $\nu N \rightarrow \nu N$ ratio at $Q^2 > 0.7 \text{ GeV}^2$ (above the Cherenkov threshold for protons in mineral oil) [15]. This result is interesting, because it should be sensitive to the strange quark contribution to the axial form factor. MiniBooNE has reported the measurement $\Delta s = 0.08 \pm 0.30$, based on a Nuance prediction [56].

The $\nu p \rightarrow \nu p/\nu N \rightarrow \nu N$ ratio was reported as a function of the MiniBooNE reconstructed nucleon kinetic energy T_{rec} . Also the migration matrices were published in Ref.[57], which carry the detector resolution and efficiency information. Using them one can smear the predicted cross-sections and obtain the predicted event rates as a function of T_{rec} . The procedure for carrying out calculations of event rates in terms of the MiniBooNE reconstructed energy is described in an Appendix of Ref.[25]. We performed the calculation of the $\nu p \rightarrow \nu p/\nu N \rightarrow \nu N$ ratio based on our neutrino interaction model and compared it to the MiniBooNE data. We have calculated our prediction of the event rates for different values of Δs covering the range from -0.4 to 0.4 . An example of the calculation is shown in Fig.8.

Using the full error matrix for the ratio published in Ref.[57] we calculated the χ^2 distribution between data and the MC. Our calculation leads to:

$$\Delta s = -0.11 \pm 0.36.$$

with $\chi^2_{min} = 33.4$ for 29 degrees of freedom. This result is consistent with all other measurements of Δs , including the one reported by MiniBooNE. We show a calculated NCE cross-section and NCE/CCQE ratio with the values of $\Delta s = -0.11$ and $M_A = 1.28 \text{ GeV}$ in Fig.7. As one can see the effect of strange quarks is small, but the agreement between data and our prediction does improve a little bit at low Q^2 region with $\Delta s = -0.11$.

IV. CONCLUSIONS

In this article we study neutral-current elastic (anti)neutrino scattering on Carbon and CH_2 targets in the framework of RDWIA approach placing particular emphasis on nuclear effects. We calculated the NCE exclusive $d\sigma/dT$ cross sections for nucleon knockout in

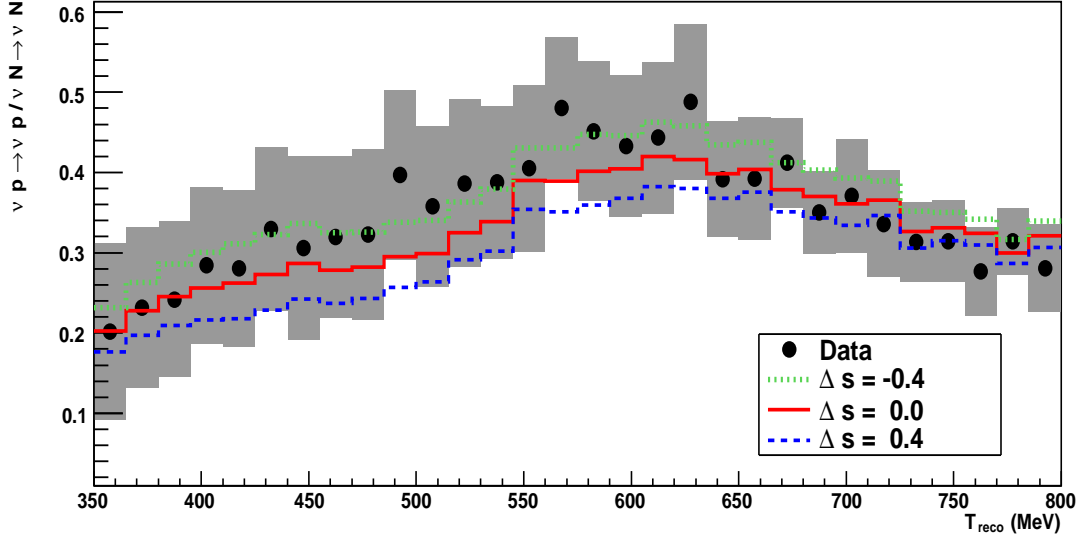


FIG. 8: (Color online). MiniBooNE $\nu p \rightarrow \nu p / \nu N \rightarrow \nu N$ ratio as a function of T_{rec} . The prediction for $\Delta s = 0.0$ and $\Delta s = 0.4$ are shown as red solid and blue dashed histograms, respectively. The MiniBooNE data are shown as points with the total error bars on top of them.

(anti)neutrino scattering on a Carbon target. The calculation presented in this paper are consistent with the RDWIA cross sections of Ref. [34, 37].

We also calculated the $d\sigma/dQ^2$ inclusive cross sections for neutrino scattering on ^{12}C , as well as, on free nucleon for different neutrino energies and estimated the range of Q^2 where nuclear effects on the shape of Q^2 distribution are negligible. We show that these effects in the CCQE and NCE scattering are similar.

Using the RDWIA approach with the Booster Neutrino Beamline flux [54] we extracted axial mass from a “shape-only” fit of the measured flux-averaged $d\sigma/dQ_{QE}^2$ differential cross section. The extracted value of $M_A = 1.28 \pm 0.05$ is in agreement within errors with the MiniBooNE result of $M_A = 1.39 \pm 0.11$ GeV. There is a good overall agreement within errors in the range of $0.25 (\text{GeV}/c)^2 < Q^2 < 1.65 (\text{GeV}/c)^2$ between RDWIA prediction and the MiniBooNE data: the measured MiniBooNE NCE flux-averaged differential cross section $d\sigma/dQ_{QE}^2$ on CH_2 and the NCE/CCQE cross section ratio. However, in the range of low $Q^2 \leq 0.25 (\text{GeV}/c)^2$ the calculations underestimate the measurements by 17% or less.

Using MiniBooNE data for the high energy $\nu p \rightarrow \nu p$ to $\nu N \rightarrow \nu N$ ratio the value of

$\Delta s = -0.11 \pm 0.36$ has been extracted based on our model, which is consistent with other measurements of Δs .

We conclude that the RDWIA approach was successfully tested against neutrino CCQE and NCE scattering on ^{12}C .

Acknowledgments

The authors greatly acknowledges to R. Tayloe and G.P. Zeller for fruitful discussions and a critical reading of the manuscript.

Appendix A: Flux-averaged NCE inclusive cross section

MiniBooNE measured the flux-averaged NCE differential cross section (per nucleon) on CH_2 , averaged over three process: scattering off free protons in Hydrogen, bound protons in Carbon, and bound neutrons in Carbon. This cross section can be expressed as

$$\frac{d\sigma_{\nu N}}{dQ_{QE}^2} = \frac{1}{7}C_{\nu p,H}\frac{d\sigma_{p,H}}{dQ_{QE}^2} + \frac{3}{7}C_{\nu p,C}\frac{d\sigma_{p,C}}{dQ_{QE}^2} + \frac{3}{7}C_{\nu n,C}\frac{d\sigma_{n,C}}{dQ_{QE}^2}, \quad (\text{A1})$$

where $d\sigma_{p,H}$ is the NCE cross section on free protons (per proton), $d\sigma_{p,C}$ is the cross section on bound protons (per proton), $d\sigma_{n,C}$ is the cross section on bound neutrons (per neutron), $C_{\nu p,H}$, $C_{\nu p,C}$, and $C_{\nu n,C}$ are the efficiency correction functions, that are given in Table IV of Ref. [15].

In this paper the NCE inclusive cross sections for neutrino ($\nu_\mu + \nu_e$) scattering on bound proton $d\sigma_p/dQ_{QE}^2$ and on bound neutron $d\sigma_n/dQ_{QE}^2$ are calculated in the RDWIA approach. The flux-averaged $\langle d\sigma/dQ_{QE}^2 \rangle$ cross section can be written as

$$\left\langle \frac{d\sigma}{dQ_{QE}^2}(Q_{QE}^2) \right\rangle = \frac{1}{\Phi} \int_{\varepsilon_{\min}}^{\varepsilon_{\max}} \frac{d\sigma_i}{dQ_{QE}^2}(Q_{QE}^2, \varepsilon_\nu) [I_{\nu_\mu}(\varepsilon_\nu) + I_{\nu_e}(\varepsilon_\nu)] d\varepsilon_\nu, \quad (\text{A2})$$

where I_{ν_μ} (I_{ν_e}) is the neutrino spectrum and Φ is the neutrino flux ($\nu_\mu + \nu_e$) in ν - mode of beam, integrated over $0 \leq \varepsilon_\nu \leq 2.6$ GeV. This definition of the flux-averaged NCE inclusive cross section is similar to the definition in Ref. [55] of the flux-integrated CCQE differential cross section $d\sigma/dQ^2$.

- [2] W. M. Alberico, S. M. Bilenky, and C. Maieron, Phys. Rept. **358**, 227 (2002).
- [3] A. O. Bazarko *et al.*, Z.Phys. **C65**, 189 (1995).
- [4] D. Adams *et al.*, Phys.Rev. **D56**, 5330 (1997).
- [5] R. D. McKeown Phys. Lett. **B219**, 140 (1989).
- [6] D. H. Beck Phys. Rev. **D39**, 3248 (1989).
- [7] K. A. Aniol *et al.*, Phys. Rev. Lett. **82**, 1096 (1999); Eur.Phys.J. **A31**, 597 (1999).
- [8] D. Spayde *et al.*, Phys. Rev. Lett. **84**, 1106 (2000); Phys. Lett. **B583**, 79 (2004).
- [9] F. E. Maas, P. Achenbach, K. Aulenbacher, S. Baunack, L. Capozza, Phys. Rev. Lett. **93**, 022002 (2004).
- [10] F. E. Maas *et al.*, Phys. Rev. Lett. **94**, 152001 (2005).
- [11] D. S. Armstrong *et al.*, Phys. Rev. Lett. **95**, 092001 (2005).
- [12] J. Liu, R. D. McKeown, and M. J. Ramsey-Musolf, Phys. Rev. **C76**, 025202 (2007).
- [13] D. S. Ahres *et al.*, Phys. Rev. **D35**, 785 (1987).
- [14] L. Bugel *et al.*, (FINeSSE Collaboration) arXiv:hep-ex/0402007.
- [15] A. A. Aguilar-Arevalo *et al.*, Phys. Rev. **D82**, 092005 (2010).
- [16] K. S. McFarland *et al.*, (MiNERvA Collaboration), Nucl. Phys. B (Proc. Suppl.) **159**, 107 (2006).
- [17] C. Athanassopoulos *et al.*, Phys. Rev. Lett. **77**, 3082 (1996).
- [18] G. L. Fogli, E. Lisi, and A. Marrone *et al.*, Phys. Rev. **D64**, 093005 (2001).
- [19] A. Donini, M. Maltoni, D. Meloni, P. Migliozi, and F. Terranova, JHEP **12**, 013 (2007).
- [20] A. Dighe and S. Ray, Phys. Rev. **D76**, 113001 (2007).
- [21] Q. R. Ahmad *et al.*, Phys. Rev. Lett. **89**, 011301 (2002).
- [22] Y. Fukuda *et al.*, Phys. Rev. Lett. **85**, 3999 (2000).
- [23] K. Abe *et al.*, Phys. Rev. Lett. **97**, 171801 (2006).
- [24] P. Adamson *et al.*, Phys.Rev. Lett. **101**, 221804 (2008); Phys. Rev. **D81**, 052004 (2010).
- [25] D. Perevalov, FERMILAB-THESIS-2009-47
- [26] O. Benhar and G. Veneziano, arXiv:nucl-th/1103.0987 (2011).
- [27] B. I. S. van der Ventel, and J. Piekarewicz, Phys. Rev. **C69**, 035501 (2004); Phys. Rev. **C73**, 025501 (2006). B. I. S. van der Ventel, and J. Piekarewicz, Phys. Rev. **C69**, 035501 (2004); Phys. Rev. **C73**, 025501 (2006).
- [28] W. M. Alberico, M. B. Barbado, S. M. Bilenky, J. A. Caballero, C. Giunti, C. Maieron,

- E. Moya de Guerra, and J. M. Udias, Nucl. Phys. **A623**, 471 (1997); Phys. Lett., **B438**, 9 (1998).
- [29] M. B. Barbado, A. De Pace, T. W. Donnelly, A. Molinari, and M. J. Musolf, Phys. Rev. **C54**, 1954 (1996)
- [30] C. Bleve, G. Co', I. De Mitri, P. Bemardini, G. Mancarella, D. Martello, and A. Surdo, Astropart. Phys. **16**, 154 (2001)
- [31] A. Botrugno, and G. Co', Nucl. Phys. **A761**, 200 (2005)
- [32] C. J. Horowitz, Hungchong Kim, D. P. Murdock, S. Pollock, Phys. Rev. **C48**, 3078 (1993)
- [33] G. T. Garvey, S. Krewald, E. Kolbe, and K. Langanke Phys. Lett. **B289**, 249 (1992).
- [34] A. Meucci, C. Giusti, and F. D. Pacati, Nucl. Phys. **A773**, 250 (2006).
- [35] A. Meucci, C. Giusti, and F. D. Pacati, Phys. Rev. **C77**, 034606 (2008).
- [36] K. S. Kim, M. K. Cheoun, and B. G. Yu, Phys. Rev. **C77**, 054604 (2008).
- [37] M. C. Martinez, P. Lava, N. Jachowicz, J. Ryckebusch, K. Vantournhout, and J. M. Udias, Phys. Rev. **C73**, 024607 (2006).
- [38] N. Jachowicz, P. Vancrayveld, P. Lava, C. Praet, and J. Ryckebusch, Phys. Rev. **C76**, 055501 (2007).
- [39] A. V. Butkevich and S. A. Kulagin, Phys. Rev. **C76**, 045502, (2007).
- [40] A. V. Butkevich, Phys. Rev. **C78**, 015501 (2008).
- [41] A. V. Butkevich, Phys. Rev. **C80**, 014610, (2009).
- [42] A. V. Butkevich, Phys. Rev. **C82**, 055501, (2010).
- [43] P. Mergell, U.-G. Meissner, and D. Drechsel, Nucl. Phys. **A596**, 367, 1996.
- [44] T. de Forest, Nucl. Phys. **A392**, 232, 1983.
- [45] D. Dutta *et al.*, Phys. Rev. **C68**, 064603, (2003).
- [46] J. J. Kelly Phys. Rev. **C71**, 064610 (2005).
- [47] C. J. Horowitz D. P. Murdock, and Brian D. Serot, in *Computational Nuclear Physics 1: Nuclear Structure* edited by K. Langanke, J. A. Maruhn, Steven E. Koonin (Springer-Verlag, Berlin, 1991), p.129
- [48] J. J. Kelly Phys. Rev. **C59**, 3256 (1999).
- [49] J. J. Kelly, <http://www.physics.umd.edu/enp/jjkelly/LEA>
- [50] E. D. Cooper, S. Hama, B. C. Clark, and R. L. Mercer, Phys. Rev. **C47**, 297 (1993).
- [51] K. G. Fissum *et al.*, Phys. Rev. **C70**, 034606, 2004

- [52] A. Meucci, F. Capuzzi, C. Giusti, and F. D. Pacati, Phys. Rev. **C67**, 054601 (2003).
- [53] A. Meucci, C. Giusti, and F. D. Pacati, Nucl. Phys. **A744**, 307 (2004).
- [54] A. A. Aguilar-Arevalo *et al.*, Phys. Rev. **D79**, 072002 (2009).
- [55] A. A. Aguilar-Arevalo *et al.*, Phys. Rev. **D81**, 092005 (2010).
- [56] D. Casper, Nucl. Phys. B, Proc. Suppl. **112**, 161 (2002).
- [57] MiniBooNE Neutral Current Elastic data release for Ref.[15], http://www-boone.fnal.gov/for_physicists/data_release/ncel